Theory of spin relaxation in two-electron laterally coupled Si/SiGe quantum dots

Martin Raith,[1] Peter Stano,[2,3] and Jaroslav Fabian[1]
[1]*Institute for Theoretical Physics, University of Regensburg, D-93040 Regensburg, Germany*
[2]*Institute of Physics, Slovak Academy of Sciences, 845 11 Bratislava, Slovakia*
[3]*Department of Physics, University of Basel, Klingelberstrasse 82, CH-4056 Basel, Switzerland*
(Received 28 June 2012; published 28 November 2012)

Highly accurate numerical results of phonon-induced two-electron spin relaxation in silicon double quantum dots are presented. The relaxation, enabled by spin-orbit coupling and the nuclei of ^{29}Si (natural or purified abundance), is investigated for experimentally relevant parameters, the interdot coupling, the magnetic field magnitude and orientation, and the detuning. We calculate relaxation rates for zero and finite temperatures (100 mK), concluding that our findings for zero temperature remain qualitatively valid also for 100 mK. We confirm the same anisotropic switch of the axis of prolonged spin lifetime with varying detuning as recently predicted in GaAs. Conditions for possibly hyperfine-dominated relaxation are much more stringent in Si than in GaAs. For experimentally relevant regimes, the spin-orbit coupling, although weak, is the dominant contribution, yielding anisotropic relaxation rates of at least two orders of magnitude lower than in GaAs.

DOI: 10.1103/PhysRevB.86.205321 PACS number(s): 72.25.Rb, 03.67.Lx, 71.70.Ej, 73.21.La

I. INTRODUCTION

Since the proposal of Loss and DiVincenzo,[1] electron spins in semiconductor quantum dots have been in the perpetual focus of research on spintronics.[2–4] In GaAs-based qubits, which are the state of the art, the essential gate operations[1,5,6] for quantum computation[7,8] have been demonstrated.[9–18] But GaAs possesses a serious handicap for coherent spin manipulations—the nuclear spins.[19,20] Controlling this source of decoherence is of major interest and an active field of research.[18,21–26]

Alternatives to III-V semiconductors with inherent nuclear spins are systems composed of atoms without nuclear magnetic moments, such as Si and C.[27–29] Natural silicon consists of three isotopes: ^{28}Si (92.2%), ^{29}Si (4.7%), and ^{30}Si (3.1%).[30] Hereof only ^{29}Si has nonzero nuclear spin ($I = 1/2$), and purification can further reduce its abundance down to 0.05%.[31,32] For this reason, silicon-based quantum dots have become the new focus of interest, and recent progress emphasizes their perspectives.[33–36] Another advantage of silicon[8,29] over GaAs is a larger g factor, which allows spin manipulations in smaller magnetic fields. On the other hand, device fabrication of silicon dots is more challenging,[37] the spin-orbit interactions are weaker, and the dots must be smaller due to a larger effective mass.

Bulk silicon has six equivalent conduction-band minima located on the Δ lines, at $k_v \approx 0.84k_0$ toward the six X points of the Brillouin zone, where $k_0 = 2\pi/a_0$ with $a_0 =$ 5.4 Å the lattice constant.[38–40] They are typically referred to as Δ valleys or X valleys. In general, their degeneracy is lifted by strain, or by the presence of an interface.[39,41] In a (001)-grown silicon heterostructure, the four in-plane valleys are split by at least 10 meV from the two lower-lying $\pm z$ valleys, resulting in a twofold conduction-band minimum. This remaining degeneracy is further split if the perpendicular confinement is asymmetric, resulting in an energy difference called the ground-state gap.[42–49] As the valley degeneracy is believed to be the main obstacle for silicon-based quantum computation,[46,50,51] a large valley splitting is desired. If this is the case, the multivalley system can be reduced to an effective single-valley qubit, a potentially nuclear-spin-free analog to the well-known GaAs counterpart.[50,51] In fact, many recent experiments performed on Si/SiGe quantum dots have no evidence of valley degeneracy,[33–35,52–54] indicating that the splitting is large enough to justify a single-valley treatment. On the other hand, a recent proposal of valley-defined qubits uses the valley degree of freedom as a tool for gate operations.[55] This requires precise control of the ground-state gap, a challenging task for the future. In this work we assume that the valley splittings are larger than the typical energy scale of interest so that the effective single-valley approximation is valid.

The spin relaxation and decoherence have been investigated theoretically and experimentally in silicon-based single and double dots from single- to many-electron occupancy.[34,35,50,53,54,56–67] Our work completes these findings by a global, quantitative understanding of two-electron lateral silicon double quantum dots. We investigate the spin-orbit and hyperfine-induced relaxation rate as a function of interdot coupling, detuning, and the magnitude and orientation of the external magnetic field for zero and finite temperatures, and for natural and isotopically purified silicon. We pay special attention to the spin hot spots,[68] and investigate individual relaxation channels. This work is an extension to the findings in Ref. 69 for GaAs, and we highlight the differences between these two materials. We fix the double-dot orientation with respect to the crystallographic axes to that which is used most often in experiments. Our choices for other parameters are similarly guided by realistic values. Although we cannot present results for the complete parametric space, by exploring most direct experimental controls we expect the presented picture of double-dot two-electron spin relaxation in Si to be exhaustive, meaning the results listed below will remain qualitatively correct also beyond the specific parameter choices we make.

We find that due to the small spin-orbit coupling the spin relaxation rates are typically at least two orders of magnitude lower than in comparable GaAs dots, and that the relaxation rate peaks at spin hot spots are very narrow in parameter space.

For detuned double dots, the energy spectrum close to the singlet-singlet anticrossing is qualitatively different from the GaAs counterpart, due to the rather small single-dot exchange coupling compared to the anticrossing energy. We also find that the hyperfine-induced relaxation rates of natural silicon are typically two and more orders of magnitude lower than the spin-orbit-induced relaxation rates. The hyperfine-induced rates of purified silicon are further suppressed by about two orders of magnitude compared to those in natural silicon. Although the anomalous regime of nuclei dominating the relaxation, which we identified in GaAs,[69] exists also in Si, here the different material parameters make it much harder to observe in practice. We therefore conclude that, concerning the relaxation, the nuclear field is negligible. Thus, the anisotropy of the spin-orbit field manifests itself in all the relaxation rates we calculated, yielding the electrically controlled directional switch of the easy passage[70] (a particular orientation of the magnetic field for which the relaxation as a function of some parameter is significantly lower than for other orientations), previously found in GaAs.[69] A temperature of 0.1 K does not change our findings in any qualitative way.

II. MODEL

We consider a ($\hat{z} = [001]$)-grown top-gated Si/SiGe heterostructure defining a laterally coupled double quantum dot within the silicon layer with a fraction of ^{29}Si isotopes. The double dot is charged with two electrons and not coupled to leads. Assuming the validity of the effective single-valley approximation,[50] the Hamiltonian in the two-dimensional and the envelope function approximation reads

$$H = \sum_{i=1,2} (T_i + V_i + H_{Z,i} + H_{\mathrm{so},i} + H_{\mathrm{nuc},i}) + H_{\mathrm{C}}. \quad (1)$$

The operators of position $\mathbf{r}$ and momentum $\mathbf{P}$ are two dimensional, where $\hat{x} = [100]$ and $\hat{y} = [010]$. The single-electron terms are labeled by the electron index i. The kinetic energy is $T = \mathbf{P}^2/2m$, with the kinetic momentum $\mathbf{P} = -i\hbar\nabla + e\mathbf{A}$, the effective electron mass m, and the electron charge $-e$. For an external magnetic field given by $\mathbf{B} = (B_\parallel \cos\gamma, B_\parallel \sin\gamma, B_z)$, where γ is the angle between the in-plane component of $\mathbf{B}$ and $\hat{x}$, the vector potential in symmetric gauge reads $\mathbf{A} = B_z(-y,x)/2$. We neglect the orbital effects of the in-plane magnetic field component, which is a good approximation up to roughly 10 T for common heterostructures.[71] The electrostatic potential,

$$V = \frac{\hbar^2}{2ml_0^4} \min\{(\mathbf{r}-\mathbf{d})^2, (\mathbf{r}+\mathbf{d})^2\} + e\mathbf{E}\cdot\mathbf{r}, \quad (2)$$

consists of the biquadratic confinement[51,72] and the external electric field. For $\mathbf{E} = 0$, the potential is minimal at $\pm\mathbf{d}$. The dimensionless ratio $2d/l_0$ will be in further called the interdot distance. The single dot scale is given by the confinement length l_0, and equivalently by the confinement energy $E_0 = \hbar^2/(ml_0^2)$. The electric field $\mathbf{E}$ is applied along the dot main axis $\mathbf{d}$, where the angle δ gives the in-plane orientation with respect to $\hat{x}$. Turning on $\mathbf{E}$ shifts the potential minima relative to each other by the detuning energy $\epsilon = 2eEd$. The geometry is plotted in Fig. 1 of Ref. 73.

The Zeeman term is $H_{\mathrm{Z}} = (g/2)\mu_{\mathrm{B}}\boldsymbol{\sigma}\cdot\mathbf{B}$, with the vector of Pauli matrices $\boldsymbol{\sigma} = (\sigma_x, \sigma_y, \sigma_z)$, the effective Landé factor g, and the Bohr magneton μ_{B}. The spin-orbit coupling, $H_{\mathrm{so}} = H_{\mathrm{br}} + H_{\mathrm{d}}$, includes the Bychkov-Rashba[3,74] and the generalized Dresselhaus Hamiltonians,[3,75–77]

$$H_{\mathrm{br}} = (\hbar/2ml_{\mathrm{br}})(\sigma_x P_y - \sigma_y P_x), \quad (3)$$

$$H_{\mathrm{d}} = (\hbar/2ml_{\mathrm{d}})(-\sigma_x P_x + \sigma_y P_y), \quad (4)$$

parametrized by the spin-orbit lengths l_{br} and l_{d}. In this work we assume interface inversion asymmetry and choose l_{br} and l_{d} of comparable strength, according to Ref. 77. The nuclear spins of ^{29}Si predominantly couple through the Fermi contact interaction[20,78,79]

$$H_{\mathrm{nuc}} = \beta \sum_n \mathbf{I}_n \cdot \boldsymbol{\sigma}\, \delta(\mathbf{R} - \mathbf{R}_n), \quad (5)$$

where β is a constant, $\mathbf{I}_n$ is the spin of the nth nucleus at the position $\mathbf{R}_n$, and $\mathbf{R} = (\mathbf{r}, z)$ is the three-dimensional electron position operator. Here we need to consider the finite extension of the wave function perpendicular to the heterostructure interface. We assume it is fixed to the ground state of a hard-wall confinement of width w. This defines the effective width,[80]

$$h_z = \left[\int dz |\psi(z)|^4\right]^{-1}, \quad (6)$$

which evaluates to $h_z = 2w/3$. Finally, the Coulomb interaction is $H_{\mathrm{C}} = e^2/4\pi\varepsilon|\mathbf{r}_1 - \mathbf{r}_2|$, with the material dielectric constant ε.

The energy relaxation is enabled by phonons, whereas spin-orbit interactions allow for a spin flip. In a (001)-grown quantum well of silicon, the electron-phonon coupling for intravalley scattering is the deformation potential of transverse acoustic (TA) and longitudinal acoustic (LA) phonons, given by[60,64,81–84]

$$H_{\mathrm{ep}} = i \sum_{\mathbf{Q},\lambda} \sqrt{\frac{\hbar Q}{2\rho V c_\lambda}} D^\lambda_{\mathbf{Q}} [b^\dagger_{\mathbf{Q},\lambda} e^{i\mathbf{Q}\cdot\mathbf{R}} - b_{\mathbf{Q},\lambda} e^{-i\mathbf{Q}\cdot\mathbf{R}}], \quad (7)$$

where

$$D^\lambda_{\mathbf{Q}} = \left(\Xi_{\mathrm{d}} \hat{\mathbf{e}}^\lambda_{\mathbf{Q}} \cdot \hat{\mathbf{Q}} + \Xi_{\mathrm{u}} \hat{\mathbf{e}}^\lambda_{\mathbf{Q},z} \hat{Q}_z\right). \quad (8)$$

The phonon wave vector is $\mathbf{Q} = (\mathbf{q}, Q_z)$, and $\hat{\mathbf{Q}} = \mathbf{Q}/Q$. The polarizations are given by[85] λ = TA1,TA2,LA, the polarization unit vector reads $\hat{\mathbf{e}}$, and the phonon annihilation (creation) operator is denoted by b ($b^\dagger$). The mass density, the volume of the crystal, and the sound velocities are given by ρ, V, and c_λ, respectively. The efficiency of the electron-phonon coupling is set by the dilatation and shear potential constants Ξ_{d} and Ξ_{u}, respectively.

We define the relaxation rate (the inverse of the lifetime T_1) as the sum of the individual transition rates to all lower-lying states. Each rate (from $|i\rangle$ to $|j\rangle$) is evaluated using Fermi's golden rule at zero temperature,

$$\Gamma_{ij} = \frac{\pi}{\rho V} \sum_{\mathbf{Q},\lambda} \frac{Q}{c_\lambda} \left|D^\lambda_{\mathbf{Q}}\right|^2 |M_{ij}|^2 \delta\left(E_{ij} - E^\lambda_{\mathbf{Q}}\right), \quad (9)$$

where $M_{ij} = \langle i|e^{i\mathbf{Q}\cdot(\mathbf{R}_1+\mathbf{R}_2)}|j\rangle$ is the matrix element of the states with energy difference E_{ij}, and $E^{\lambda}_{\mathbf{Q}}$ is the energy of a phonon with wave vector $\mathbf{Q}$ and polarization λ. In this work we focus on the singlet (S) and the three triplets (T_-, T_0, T_+) at the bottom of the energy spectrum.

Our numerical method is discussed in Refs. 86. The extension to include the hyperfine coupling, Eq. (5), was introduced in Ref. 69. In this work, the two-electron basis for the configuration-interaction method consists of 1156 Slater determinants, generated by 34 single-electron orbital states. The discretization grid is typically 135×135. The relative error for energies is below 10^{-5}. The reliability of our code is confirmed by the evaluation of Eq. (9) in an analytically solvable regime—weakly coupled dots in low magnetic fields. For details of this calculation, see Appendix A.

We use the parameters of a SiGe/Si/SiGe quantum well grown along the $\hat{z} = [001]$ direction with a germanium concentration of 25%. The two-dimensional electron gas is defined in the thin silicon layer with tensile strain.[38,87] The in-plane effective mass is isotropic, given by the transverse mass of the X valley states,[41] and we use $m = 0.198m_e$,[88] where m_e is the free-electron mass. The effective Landé factor is $g = 2$.[44,89] Other material parameters read $c_l = 9150$ m/s (for LA phonons), $c_t = 5000$ m/s (for TA phonons), $\rho = 2330$ kg/m^3, and $\varepsilon = 11.9\varepsilon_0$.[90] The choice of deformation potential constants is not unique,[83,84,91] and we use $\Xi_d = 5$ eV and $\Xi_u = 9$ eV according to Ref. 90. The hyperfine-coupling parameter reads $\beta = -0.05$ μeV nm^3, and ^{29}Si has spin $I = 1/2$. For natural silicon, the ^{29}Si abundance is 4.7%, and we use an abundance of 0.01% for purified silicon. For the spin-orbit coupling strength we choose $l_{br} = 38.5$ μm and $l_d = 12.8$ μm.[77,89] The confinement length is $l_0 = 20$ nm ($E_0 = 1.0$ meV), in line with realistic dot sizes.[53,92] The double dot is oriented as $\mathbf{d} \,||\, [110]$. The magnetic field is in plane unless stated otherwise.

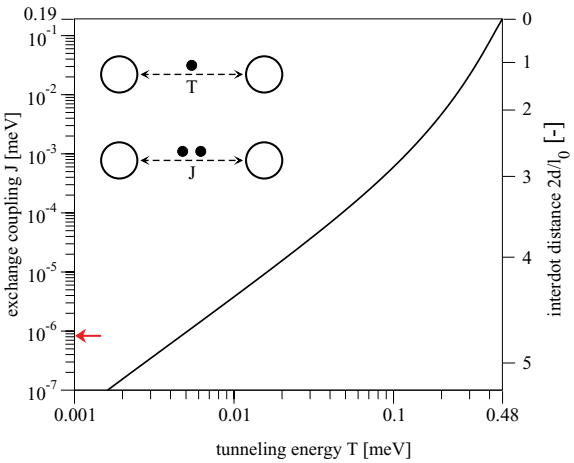

FIG. 1. (Color online) Calculated conversion between the single-electron tunneling energy T (x axis), the two-electron exchange coupling J (left y axis), and the interdot distance $2d/l_0$ (right y axis), neglecting nuclear spins. The arrow gives E_{nuc}, Eq. (10), of natural silicon.

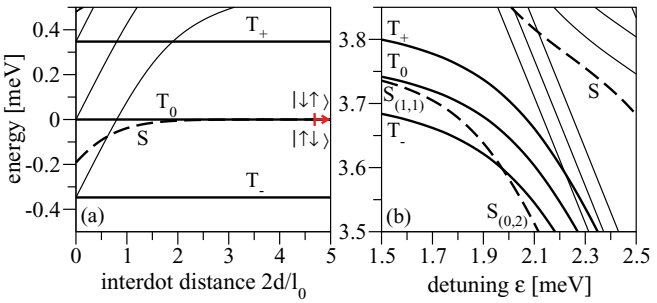

FIG. 2. (Color online) Calculated energies of the lowest states, varying (a) the interdot coupling (at $B = 3$ T) and (b) the detuning (at $B = 0.5$ T, $2d/l_0 = 2.85$). Singlet states are given by dashed and triplets by solid lines. In (a), the energy of T_0 is subtracted, and in (b), the quadratic trend in E is subtracted. The arrow in (a) marks where $J = E_{nuc}$ (for natural silicon).

III. RESULTS: UNBIASED DOUBLE DOT

We parametrize in our model the coupling of the double quantum dot by the dimensionless interdot distance $2d/l_0$. The corresponding experimental observables are the tunneling energy T (single-electron occupancy) and the exchange coupling J (two-electron occupancy). The conversion between these three equivalent parameters is plotted in Fig. 1 for clarity.

The numerically calculated energy spectrum of the unbiased double dot is shown in Fig. 2. In this section, we choose a magnetic field of $B = 3$ T. For the single dot ($d = 0$) the exchange coupling $J = E(T_0) - E(S)$ is $J_{SD} = 0.19$ meV. The Zeeman energy $E_Z = g\mu_B B$ exceeds J for magnetic fields beyond 1.7 T. Consequently, we find in Fig. 2(a) that T_- is the ground state for all interdot distances. The singlet therefore has an anticrossing with an excited triplet in the strong-coupling regime, here at $J = 75$ μeV for our choice of parameters. This scenario is hardly met in comparable GaAs double quantum dots, because the required magnitude of the magnetic field is above 10 T. The silicon spectrum resembles the GaAs spectrum for magnetic fields below 1.7 T.

At large interdot distances, the hyperfine coupling induces a splitting of S and T_0, given by

$$E_{nuc} = 2\sqrt{\left|\sum_{i=1,2}\langle\phi_a T_0|H_{nuc,i}|\phi_s S\rangle\right|^2}. \qquad (10)$$

In this regime, the lowest eigenstates are $|\uparrow\downarrow\rangle = (S + T_0)/\sqrt{2}$ and $|\downarrow\uparrow\rangle = (S - T_0)/\sqrt{2}$ (see Fig. 3). We evaluate Eq. (10) by averaging over random nuclear spin ensembles, and obtain $E_{nuc} \approx 1$ neV for natural and $E_{nuc} \approx 0.04$ neV for purified silicon. This implies a crossover to the nuclear-dominated regime at $2d/l_0 \gtrsim 4.7$ [red arrows in Figs. 1, 2(a), and 3] for natural and at $2d/l_0 \gtrsim 5.4$ for purified silicon.

We plot the relaxation rates of the states S, T_0, and T_+, denoted in Fig. 2, as functions of the interdot distance and in-plane magnetic field orientation in Fig. 4. We also give the relaxation rates of individual channels for the two principal axes, that is, for the in-plane magnetic field components parallel and perpendicular to the dot main axis $\mathbf{d}$, in the upper and lower panels of Fig. 5, respectively. We find that the relaxation rate of the singlet is highly anisotropic,[93] which can

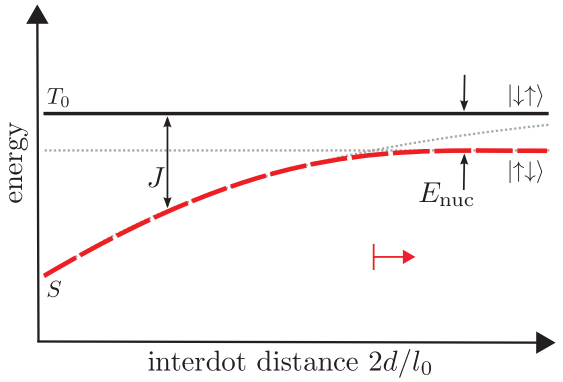

FIG. 3. (Color online) Schematic energy spectrum of an unbiased double dot showing the singlet S (dashed line) and the triplet T_0 (solid line). For large interdot distances, the exchange coupling J is given by the hyperfine splitting $E_{\rm nuc}$, Eq. (10), and the eigenstates change to $|\downarrow\uparrow\rangle$ and $|\uparrow\downarrow\rangle$.

be explained by introducing an effective spin-orbit magnetic field (see below). The rates are minimal if $\mathbf{B} \parallel \mathbf{d}$, reaching the

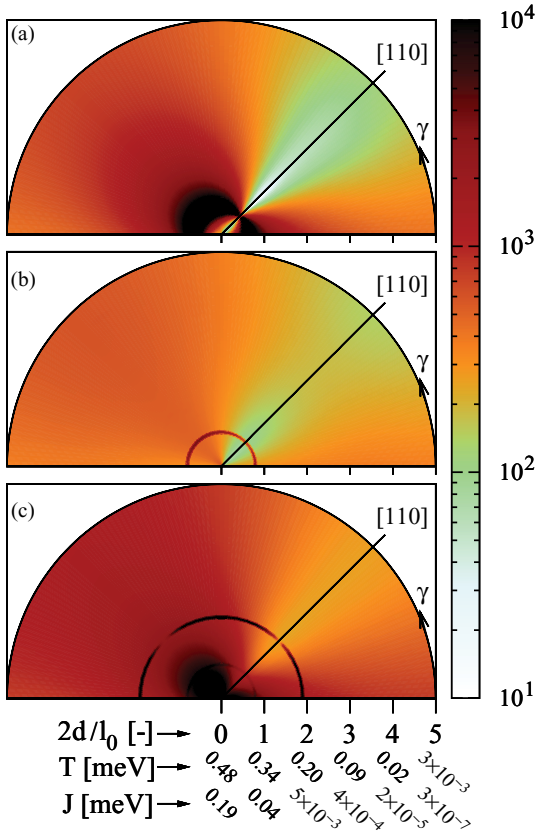

FIG. 4. (Color online) Calculated relaxation rates of (a) the singlet, (b) the triplet T_0, and (c) the triplet T_+ as functions of the in-plane magnetic field orientation γ (angle) and the interdot distance $2d/l_0$ (radius of the polar plot), for a double dot at $B = 3$ T. The x and y axes correspond to crystallographic axes [100] and [010], respectively. The dot orientation $\mathbf{d}$ || [110] is marked by a line. The x axis is converted to the tunneling energy T and the exchange J, in addition to $2d/l_0$. The rate is given in inverse seconds by the color scale. The system obeys C_{2v} symmetry, so point reflection would complete the graphs.

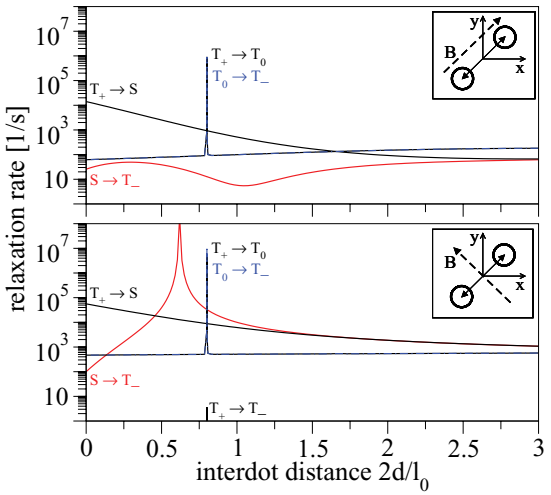

FIG. 5. (Color online) Calculated channel resolved relaxation rates vs interdot distance for both parallel (top) and perpendicular (bottom) to $\mathbf{d}$ in-plane magnetic field orientation ($B = 3$ T). The relaxation channels of T_+ are black, of T_0 are blue, and of S are red.

order of tens of milliseconds for any dot coupling strength (Fig. 5). We call this characteristic an easy passage.[70,94] In the strong-coupling regime, the rate away from the easy passage is enhanced by orders of magnitude. This results from the coupling of the singlet with the excited triplet, which favors the transition into T_-. For $\mathbf{B} \parallel \mathbf{d}$, the rate at the anticrossing is extremely sensitive to variations of γ, such that the easy passage becomes very narrow.

The relaxation rate of T_0 is given in Fig. 4(b). We find the same general anisotropic behavior, which is that the rate is minimal for $\mathbf{B} \parallel \mathbf{d}$. Figure 5 shows that the dominant channel of the relaxation is the transition $T_0 \to T_-$. Consequently, there is no impact from the singlet-triplet anticrossing. However, the anticrossing of the excited triplet with T_0 manifests itself in a very sharp peak of its rate. This spike is also anisotropic, with a difference of roughly one order of magnitude [not visible in Fig. 4(b) due to its resolution].

Figure 4(c) shows the relaxation rate of T_+. In addition to the anisotropic background, there are two spikes of enhanced rate generated by the anticrossings of T_+ with the excited triplets. The enhancement close to the single-dot regime originates from the dominant $T_+ \to S$ transition (see Fig. 5). Interestingly, the anticrossing of the singlet hardly influences the overall trend of this relaxation channel.

We plot in Fig. 6 the relaxation rates of a weakly coupled double dot as a function of in-plane magnetic field. Here we find the same qualitative behavior for all three panels. As in Fig. 4, the relaxation rate is minimal for $\mathbf{B} \parallel \mathbf{d}$, but there are no spin hot spots here.

IV. RESULTS: BIASED DOUBLE DOT

In this section we consider a weakly coupled double dot with a finite detuning energy ϵ. Figure 7 introduces important characteristic energies in a schematic energy spectrum. The state charge character is given in parentheses: (1,1) indicates that there is one electron in each dot, and (0,2) states that both electrons are in the same dot. In the spectra, we subtract

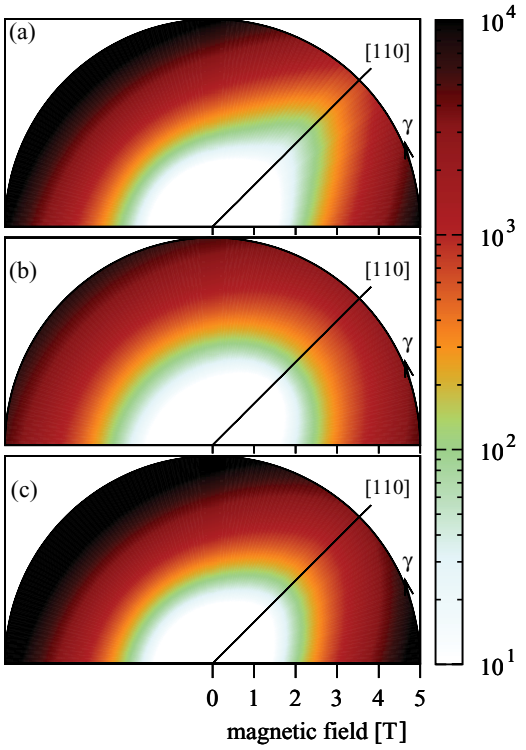

FIG. 6. (Color online) Calculated relaxation rates of (a) the singlet, (b) the triplet T_0, and (c) the triplet T_+ as functions of the in-plane magnetic field orientation γ (angle) and the magnetic field magnitude (radius of the polar plot), for a double dot with $T = 0.1$ meV. The layout with respect to the crystallographic axes is the same as in Fig. 4. The rate is given in inverse seconds by the color scale.

the quadratic trend in the electric field E. In this way, the (1,1) states are displayed horizontally unless influenced by anticrossings. The important quantities are the single-dot exchange coupling $J_{\rm SD}$, the double-dot exchange coupling J, and the singlet and triplet anticrossing energy splittings, labeled in Fig. 7. The single-dot exchange coupling $J_{\rm SD}$ is set by the material parameters, i.e., the Coulomb interaction, and the system parameters, i.e., the confinement length. For noninteracting electrons, $J_{\rm SD}$ is equal to the confinement energy E_0,

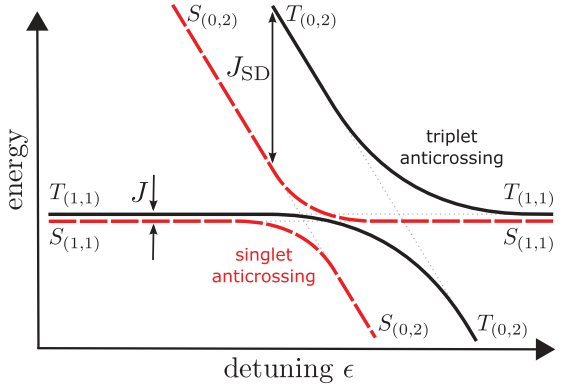

FIG. 7. (Color online) Schematic energy spectrum of a biased double dot without magnetic field. The singlets are given in dashed lines, the triplets in solid lines.

here 1 meV. For interacting particles, the Coulomb repulsion has strong impact on the symmetric ground state, the singlet, as here the electrons tend to group together. The first excited state, the triplet, is antisymmetric with respect to point reflection at the dot origin, and therefore less affected. As a consequence, $J_{\rm SD}$ *decreases as the Coulomb interaction strength increases*. For our choice of parameters $J_{\rm SD} = 0.19$ meV. In contrast, $J_{\rm SD}$ *increases as the confinement length decreases*. For instance, a confinement length of $l_0 = 17$ nm results in $J_{\rm SD} \approx 0.3$ meV. This can be understood as follows.[95] On the one hand, a stronger confinement increases the Coulomb strength due to smaller effective particle distances $|\mathbf{r}_1 - \mathbf{r}_2|$ in $H_{\rm C}$. This is an effect somewhat linear in l_0^{-1}. Then, one could expect $J_{\rm SD}$ to decrease. However, the confinement energy E_0 scales as l_0^{-2}, by which the exchange coupling increases in a similar way. This scaling dominates, such that the single-dot exchange coupling increases. The double-dot exchange coupling J decreases exponentially with increasing interdot distance d.[96] In the weak-coupling regime it holds that $J \ll J_{\rm SD}$, and we choose d such that $J = 0.6\,\mu$eV. The anticrossing gap of a spin-alike pair of states at the (1,1) $\leftrightarrow$ (0,2) transition depends on the interdot distance as well. For increasing d (decreasing J), these gaps decrease, that is, the anticrossings vanish as $2d/l_0 \to \infty$.

The numerically calculated energy spectrum is plotted in Fig. 2(b) for a magnetic field of $B = 0.5$ T. The spectrum is qualitatively different from the GaAs double-dot counterpart (see Fig. 1 in Ref. 69). In a comparable GaAs double dot, the singlet and triplet anticrossings gaps are small compared to the single-dot exchange coupling. Consequently, the singlet anticrossing is well separated from the triplet anticrossing, and the excited singlet is close to T_0 between these anticrossings.

We plot the relaxation rates of the detuned double dot in Fig. 8. Figure 8(a) corresponds to the first excited state, that is, S for detuning energies up to 1.97 meV, and T_- beyond. At the singlet-triplet anticrossing, the relaxation rate is very low as the transferred energy becomes very small. The easy passage occurs if the external, in-plane magnetic field is perpendicular to $\mathbf{d}$. The same anisotropy is visible for the relaxation rates of T_0 and T_+, Figs. 8(b) and 8(c), respectively. There is no signature of the singlet-triplet anticrossing in the rate because of the exact compensation of individual relaxation channels. Also, there is no indication of the crossing of T_+ with the excited triplet T_-. This rate behavior—anisotropies, easy-passage directional switch, and the exact compensation—is analogous to a GaAs dot and we refer the reader to Ref. 69 for a detailed discussion and explanation. Other anticrossings with excited triplets (at $\epsilon \approx 2.47$ meV) manifest themselves in extremely narrow peaks of the rate, not visible in Fig. 8 at the current resolution.

Let us comment on the possible effects of nuclear spins. Comparing the interaction strengths with the spin-orbit fields, the former are expected to be negligible. Indeed, the Overhauser field characterizing the fluctuating collective nuclear field[20]

$$\mathbf{B}_{\rm nuc} = \frac{\beta}{g\mu_{\rm B}} \left\langle \sum_n \mathbf{I}_n |\psi(\mathbf{R}_n)|^2 \right\rangle \tag{11}$$

of natural silicon is of the order of tens of μT; for purified silicon even one order of magnitude lower. On the other hand,

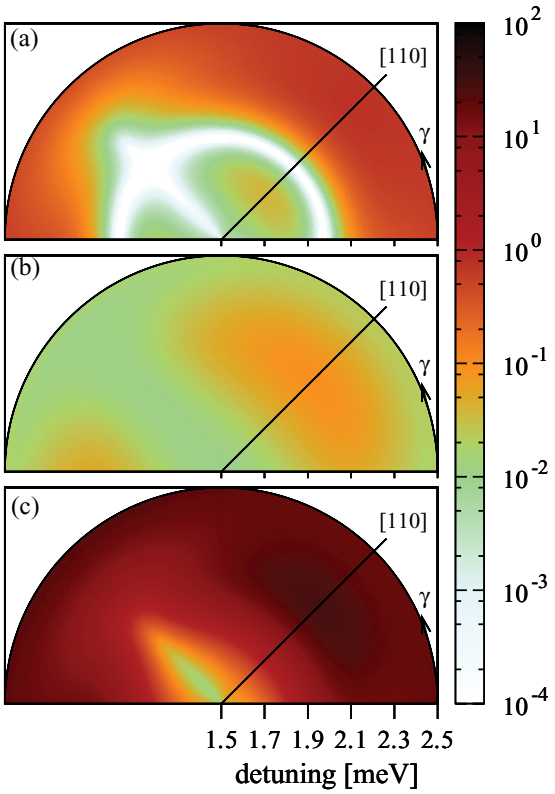

FIG. 8. (Color online) Calculated relaxation rates of (a) the first excited state [S or T_-; see Fig. 2(b)], (b) T_0, and (c) T_+ as functions of the in-plane magnetic field orientation γ (angle) and detuning energy (radius of the polar plot), for a double dot with $2d/l_0 = 2.85$ ($T = 0.1$ meV) and $B = 0.5$ T. The layout with respect to the crystallographic axes is the same as in Figs. 4 and 6. The rate is given in inverse seconds by the color scale.

the effective spin-orbit field $[x_d, y_d = (x \pm y)/\sqrt{2}]$,[70]

$$\mathbf{B}_{\rm so} = \mathbf{B} \times \left\{ x_d \left(l_{\rm br}^{-1} - l_{\rm d}^{-1} \right) [1\bar{1}0] + y_d \left(l_{\rm br}^{-1} + l_{\rm d}^{-1} \right) [110] \right\} / \sqrt{2}, \tag{12}$$

is about 2 mT at $B = 1$ T. Still, in GaAs we have found that despite a similar discrepancy, there are cases where the nuclear field dominates the spin-orbit field, as the latter is quenched by symmetry-imposed selection rules.[69] Here, such a situation arises, in principle, too. However, due to the differences in material parameters, it requires an extremely weakly coupled double dot (J of the order of sub-peV; see Appendix B for details), usually not pursued in experiments. The matrix elements of the spin-flipping transitions are in Si therefore dominated by the spin-orbit fields, rather than nuclear spin fields, and the same holds for anticrossing gaps. An illustration is given in Fig. 9.

The second possibility we considered was a dot detuned so far (such small J) that the singlet and triplet T_0 become degenerate with respect to $E_{\rm nuc}$. The Hamiltonian eigenstates change from entangled states into separable states with spin up or down in the left or right dot, respectively (we show this schematically in Fig. 3). The figures in Sec. III cover this regime but the qualitative change in the eigenstate character has no visible effects on the relaxation rates (verified also for $2d/l_0 > 5$; not shown). This is because the relaxation to

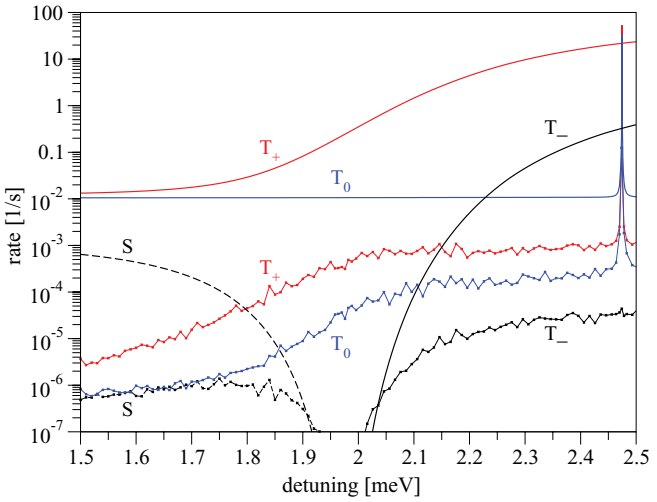

FIG. 9. (Color online) Calculated relaxation rates of a detuned double dot in an in-plane magnetic field ($B = 0.5$ T, $\gamma = 3\pi/4$) as a function of detuning. The straight lines give the spin-orbit-induced relaxation, the wiggly lines the hyperfine-induced relaxation rates (natural silicon).

a fully spin-polarized final state T_+ from the initial state S or T_0 (or any of their superpositions, such as $|{\uparrow\downarrow}\rangle$) proceeds through an individual single-dot spin flip, with the transition matrix element magnitude being essentially the same in all these cases.

Next we considered direct transitions due to random nuclear fields without phonon assistance. Such transitions are possible if the eigenstates have unsharp energies (finite lifetimes). As the states we are interested in are low lying, even at finite temperature their energy broadening is so small that the resulting nuclear-induced spin relaxation is negligible.

Finally, we considered the consequences of the random character of the nuclear field, which blurs the electron energies. This statistical, rather than quantum-mechanical, uncertainty can be grasped roughly by convoluting the relaxation curves with a Gaussian with an appropriate width, depending on which parameter we change, defined ultimately by the energy $g\mu_{\rm B}\mathbf{B}_{\rm nuc}$. We find this width to be unnoticeably small—as an example, the extremely narrow peaks in Fig. 5 survive practically untouched by such smoothing. We therefore conclude that unpolarized nuclear spins in natural or purified Si are not expected to be visible in the electron spin relaxation within the parametric space we investigate. We find that such a situation might occur only for very small external fields ($B \leqslant 0.01$ T) or very weakly coupled dots ($J \leqslant$ peV).

The figures presented and results discussed in this article were for zero temperature. In our model, a finite temperature amounts solely to allowing for energy-increasing transitions (phonon absorption), in addition to the phonon emission processes only which are present at zero temperature. We analyzed this possibility, adopting a typical experimental value of 100 mK. We have not found any case where such additional transitions would change the relaxation rates in any significant way (figures not shown). Our conclusion from these investigations is that the relaxation character, most notably its

anisotropies, will not be influenced by experimentally relevant subkelvin temperatures.

ACKNOWLEDGMENTS

This work was supported by DFG under Grant No. SPP 1285 and SFB 689. P.S. acknowledges support by meta-QUTE ITMS NFP Grant No. 26240120022, CE SAS QUTE, EU Project Q-essence, APVV-0646-10, and SCIEX.

APPENDIX A: ANALYTICAL CALCULATION OF RELAXATION RATES

In this section we analytically calculate the relaxation rate Eq. (9), adopting several approximations. The calculations prove useful to explain the physical mechanism and to verify our numerical results. The validity of the approximations will be discussed afterwards. In the following, the hyperfine coupling is neglected.

Approximating the sum in Eq. (9) by an integral, and rewriting the δ function with respect to the z component of $\mathbf{Q}$, we obtain ($i \neq j$)

$$\Gamma_{ij} = \frac{E_{ij}}{8\pi^2\rho\hbar^2}\sum_\lambda \int d\mathbf{q}\int dQ_z\,\frac{Q}{c_\lambda^3\bar{Q}_z^\lambda}\left|D_{\mathbf{Q}}^\lambda\right|^2|M_{ij}|^2 \times\left[\delta\left(Q_z-\bar{Q}_z^\lambda\right)+\delta\left(Q_z+\bar{Q}_z^\lambda\right)\right], \tag{A1}$$

where $\bar{Q}_z^\lambda = \sqrt{E_{ij}^2/(\hbar^2c_\lambda^2)-q^2}$. Assuming the validity of the dipole approximation, the matrix element reads

$$M_{ij} \approx i\langle i|\mathbf{q}\cdot(\mathbf{r}_1+\mathbf{r}_2)|j\rangle, \tag{A2}$$

where $|i\rangle$ and $|j\rangle$ are the spin-orbit-coupled two-electron eigenstates. Note that the contribution of the wave function overlap along the z direction in M_{ij} is about 1,[94] which is consistent with the two-dimensional approximation. We restrict ourselves to weakly coupled double dots, i.e., $d \gg l_0$, and incorporate the effect of spin-orbit coupling perturbatively via a Schrieffer-Wolff transformation.[97–99] The eigenstates then read (l labels the electrons)

$$|i\rangle = e^{-iO}\left(|i\rangle_0+\sum_k\sum_{l=1,2}\frac{{}_0\langle k|\bar{H}_{\mathrm{so},l}|i\rangle_0}{E_i^0-E_k^0}|k\rangle_0\right), \tag{A3}$$

with the transformation operator $O=-\sum_l \mathbf{n}_{\mathrm{so},l}\cdot\boldsymbol{\sigma}_l/2$, where

$$\mathbf{n}_{\mathrm{so},l} = \left(\frac{x_l}{l_\mathrm{d}}-\frac{y_l}{l_\mathrm{br}},\frac{x_l}{l_\mathrm{br}}-\frac{y_l}{l_\mathrm{d}},0\right), \tag{A4}$$

and the effective spin-orbit operator $\bar{H}_{\mathrm{so},l} = \bar{H}^Z_{\mathrm{so},l}+\bar{H}^{(2)}_{\mathrm{so},l}$, where

$$\bar{H}^Z_{\mathrm{so},l} = \frac{g}{2}\mu_\mathrm{B}(\mathbf{n}_{\mathrm{so},l}\times\mathbf{B})\cdot\boldsymbol{\sigma}_l, \tag{A5}$$

$$\bar{H}^{(2)}_{\mathrm{so},l} = \frac{\hbar}{4m}\left(\frac{1}{l_\mathrm{d}^2}-\frac{1}{l_\mathrm{br}^2}\right)L_{z,l}\sigma_{z,l}+\mathrm{const.} \tag{A6}$$

Here, $L_z = l_z+(e/2)r^2B_z$, where l_z is the operator of angular momentum. The states in Eq. (A3) labeled with subscript 0 are eigenstates of the Hamiltonian

$$H^0 = \sum_{i=1,2}(T_i+V_i+H_{Z,i})+H_\mathrm{C}; \tag{A7}$$

their eigenenergies are denoted as E^0. We use the Heitler-London ansatz[100] to approximate the eigenstates of Eq. (A7).

We use Eq. (A3) to evaluate the matrix element M_{ij}. It is straightforward to show that contributions from coupling within the lowest four-dimensional subspace $\mathcal{M} = \{S,T_-,T_0,T_+\}$ are zero or exponentially suppressed in d/l_0. As a result, the relaxation requires coupling via higher states. Neglecting the L_z contribution to the effective spin-orbit coupling Eq. (A6), we obtain

$$\frac{M_{ij}}{ig\mu_\mathrm{B}} = \sum_{k\notin\mathcal{M}}\sum_{l=1,2}\left[\frac{{}_0\langle i|(\mathbf{n}_{\mathrm{so},l}\times\mathbf{B})\cdot\boldsymbol{\sigma}_l|k\rangle_0}{E_i^0-E_k^0}{}_0\langle k|q_xx_1+q_yy_1|j\rangle_0 + \frac{{}_0\langle k|(\mathbf{n}_{\mathrm{so},l}\times\mathbf{B})\cdot\boldsymbol{\sigma}_l|j\rangle_0}{E_j^0-E_k^0}{}_0\langle i|q_xx_1+q_yy_1|k\rangle_0\right]. \tag{A8}$$

The singlet is symmetric with respect to the inversion operator I (point reflection in real space), the triplets are antisymmetric.[86] Consequently, it follows from Eq. (A8) that, within the dipole approximation, the singlet-triplet transition is forbidden. We also find that Eq. (A8) forbids a $T_+ \leftrightarrow T_-$ transition because the effective spin-orbit operator $\bar{H}^Z_{\mathrm{so},l}$ acts on only one of the two electron spins. Let us now look at the transition between T_0 and $T_\pm$.

To evaluate Eq. (A8), we reduce the infinite sum over k to cover only states within the energy window of about the confinement energy, $\hbar^2/(ml_0^2)$. Additionally, we can exclude any singlet from the sum, because the electron-phonon operator does not act in spin space. What is left can be captured by the Heitler-London approach.

Let $|\mathrm{R0}\rangle$ be the (orbital) ground state of a single dot shifted to the "right" by d, i.e., the Fock-Darwin state of the right dot with the principal quantum number $n=0$ and the orbital quantum number $l=0$. Analogously we define the ground state of the "left" dot. The properly symmetrized triplet lowest in energy is

$$|\Psi_T\rangle_0 = (|\mathrm{R0,L0}\rangle-|\mathrm{L0,R0}\rangle)\otimes|T\rangle/\sqrt{2}. \tag{A9}$$

The orbitally excited triplets can be constructed analogously, using $|\mathrm{R1}\rangle$, and $|\mathrm{L1}\rangle$, the displaced Fock-Darwin states with $n=0$ and $|l|=1$:

$$|k_\pm\rangle_0 = (|\mathrm{R0,L1}\rangle-|\mathrm{L1,R0}\rangle\pm(|\mathrm{R1,L0}\rangle-|\mathrm{L0,R1}\rangle)) \otimes|T\rangle/2. \tag{A10}$$

Neglecting the wave function overlap of states localized in different quantum dots, we calculate the matrix elements ${}_0\langle\Psi_T|x_1|k_\pm\rangle_0$ and ${}_0\langle\Psi_T|y_1|k_\pm\rangle_0$ analytically, yielding

$${}_0\langle\Psi_T|x_1|k_+\rangle_0 = l_0/\sqrt{8}, \tag{A11}$$

$${}_0\langle\Psi_T|y_1|k_+\rangle_0 = \mathrm{sgn}(l)\mathrm{i}l_0/\sqrt{8}, \tag{A12}$$

and ${}_0\langle\Psi_T|x_1|k_-\rangle_0 = {}_0\langle\Psi_T|y_1|k_-\rangle_0 = 0$. We use Eqs. (A11) and (A12) as an approximation for the matrix elements in Eq. (A8). We also require the matrix elements of Pauli matrices

respecting the spin quantization axis along **B**. They read

$$\langle T_\pm|\boldsymbol{\sigma}_1|T_0\rangle = \frac{e^{\mp i\gamma}}{2\sqrt{2}}\begin{pmatrix}\cos(\gamma-\theta)+\cos(\gamma+\theta)\pm 2i\sin(\gamma)\\ \sin(\gamma-\theta)+\sin(\gamma+\theta)\mp 2i\cos(\gamma)\\ 2\sin(\theta)\end{pmatrix}, \tag{A13}$$

where $\theta=\cos^{-1}(B_z/B_\parallel)$. The energy differences in Eq. (A8) are approximated by the confinement energy $\hbar^2/(ml_0^2)$.

With these ingredients, we can solve Eq. (A1), integrating over the phonon momentum, and obtain

$$\Gamma_{T_0\to T_-}=\Gamma_{T_+\to T_0}=\frac{m^2 l_0^8\mathcal{L}_{\rm so}^{-2}}{12\pi\rho\hbar^{10}}(g\mu_{\rm B}B)^7 \times\left[c_l^{-7}\left(\frac{3}{35}\Xi_{\rm u}^2+\frac{2}{5}\Xi_{\rm u}\Xi_{\rm d}+\Xi_{\rm d}^2\right)+c_t^{-7}\frac{4}{35}\Xi_{\rm u}^2\right], \tag{A14}$$

with the effective spin-orbit length $\mathcal{L}_{\rm so}$ defined by

$$\mathcal{L}_{\rm so}^{-2}=\begin{cases}2\left(l_{\rm br}^{-2}+l_{\rm d}^{-2}\right) & \text{if } \theta=0,\\ l_{\rm br}^{-2}+l_{\rm d}^{-2}-2\frac{\sin(2\gamma)}{l_{\rm br}l_{\rm d}} & \text{if } \theta=\pi/2.\end{cases} \tag{A15}$$

Now we discuss the validity of the approximations used during the derivation of Eq. (A14). The matrix element M_{ij} is calculated using the dipole approximation Eq. (A2). It requires that the energy difference between the transition states, here T_0 and $T_\pm$, fulfills $E_{ij}\ll\hbar c_\lambda/l_0$.[94] Using $E_{ij}=g\mu_{\rm B}B$ and $c_\lambda=c_t$, we obtain the condition $B\ll 1.4$ T. We consider also a weakly coupled double dot, $d\gg l_0$, to comply with most experiments. This limit ensures negligible matrix elements among the states of $\mathcal{M}$, and justifies the Heitler-London approximation. Here, the spectrum also develops bundles of eigenenergies separated by the confinement energy $\hbar^2/(ml_0^2)$, a fact used to approximate the energy differences in Eq. (A8). Note that within the restriction of the dipole approximation ($B\ll 1.4$ T), the Zeeman energy ($E_{\rm Z}\ll 0.16$ meV) is negligible compared to the confinement energy ($E_0=1$ meV). The Schrieffer-Wolff transformation is the essential tool for a perturbative treatment of spin-orbit coupling in the double dot.[101] Perturbation theory with the unitarily transformed Hamiltonian yields results which are higher order in small quantities compared to the original Hamiltonian.[93,101] Finally, we note that, since L_z is symmetric with respect to the inversion I, the perturbation $\bar{H}^{(2)}_{{\rm so},l}$, Eq. (A6), vanishes for all transitions $T_0\leftrightarrow T_\pm$.

We compare the analytical formula for the relaxation rate of the transition $T_0\to T_-$, and $T_+\to T_0$, given in Eq. (A14), with the numerical results in Fig. 10. We find perfect agreement for low magnetic fields, in line with the condition $B\ll 1.4$ T. For larger magnetic fields, the results significantly deviate from the B^7 power law, due to the breakdown of the dipole approximation. We also find that the $S\leftrightarrow T_\pm$ relaxation channels, which we found to be zero in the lowest-order dipole approximation due to their symmetry, show B^9 dependence, indicating that the relaxation is driven by the second-order term of **q**. Being of higher order, the relaxation rate, for small **B**, is at least one order of magnitude lower than the $T_0\leftrightarrow T_\pm$ transitions.

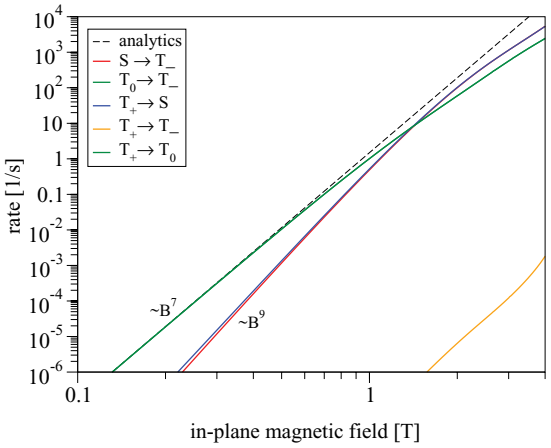

FIG. 10. (Color online) Calculated relaxation rates of individual transition channels as a function of in-plane magnetic field for a weakly coupled quantum dot. The magnetic field is oriented along $[\bar{1}10]$ ($\gamma=3\pi/4$) and the dots along [110] ($\delta=\pi/4$). The interdot distance is $2d/l_0=2.85$, yielding the tunneling energy $T=0.1$ meV. The dashed, black line gives the analytical relaxation rate, evaluated with Eq. (A14).

APPENDIX B: NUCLEAR DOMINANCE

Here we estimate the parameters at which, for the electron spin relaxation, nuclear spins dominate the spin-orbit fields. Comparing the strengths of the two effective fields, as is done in the main text, one does not expect such a situation to arise, unless at very small (below 10 mT or so) external magnetic fields. This regime is not usually met in experiments, where a sizable Zeeman splitting is necessary for electron spin manipulations and measurements. We have found in our previous work on GaAs quantum dots[69] that, despite the discrepancy, there are anomalous cases where the above expectation fails and nuclei are indeed the dominant channel. This happens in a weakly coupled double dot biased to the $S_{1,1}$-$S_{0,2}$ anticrossing, if the corresponding anticrossing gap $E_{S\text{-}S}$ is small enough. Namely, due to the absence of the spin-orbit coupling between states T_0 and S, the small magnitude of the nuclear-induced wave function admixture is compensated by the small energetic distance apart of the two states. The very same mechanism is also present in Si, raising the question of the conditions needed for it to become manifest.

We will illustrate the case by comparing Si to GaAs. For this, we assume that the single-dot energy E_0 and the Zeeman energy are the same in the two quantum dots, each built in one of the two materials. We estimate the ratio of the exchange energies (which characterize the interdot coupling) below for which the nuclei dominate. As described above, this happens if

$$g\mu_{\rm B}B_{\rm nuc}/E_{S\text{-}T}\gtrsim g\mu_{\rm B}B_{\rm so}/E_{T\text{-}T}, \tag{B1}$$

where the effective magnetic fields are defined in Eqs. (11) and (12), $E_{S\text{-}T}$ is the difference between the energies of the states S and T_0, approximately equal to the $S_{1,1}$-$S_{0,2}$ anticrossing gap, and $E_{T\text{-}T}$ is the energy difference between the state T_0 and the closest excited triplet, which we approximate by the orbital energy scale E_0. We define a "critical" $E_{S\text{-}T}$ energy difference by Eq. (B1) with an equality sign. Approximating the two

electron wave functions by Slater determinants composed of localized Fock-Darwin states of a single dot, we get the following auxiliary results, valid for large interdot distances:

$$E_{S\text{-}S} \approx \frac{e^2}{\sqrt{2}\epsilon_0\epsilon_r d}\exp(-d^2/l_0^2) \tag{B2}$$

and

$$J \approx \exp(-2d^2/l_0^2)\frac{4d}{\sqrt{\pi}l_0}\frac{\hbar^2}{ml_0^2}. \tag{B3}$$

Both of these quantities fall off exponentially with increasing interdot distance in weakly coupled dots. However, the S-S anticrossing gap scales as the tunneling energy T, whereas the exchange energy is much smaller, $J \sim T^2/U$ (here U is the charging energy).[102] With these we get for the ratio of critical exchange energies

$$\frac{J_{\text{crit}}^{\text{Si}}}{J_{\text{crit}}^{\text{GaAs}}} \sim \left(p\frac{(I\beta l_{\text{so}}\epsilon_r)_{\text{Si}}}{(I\beta l_{\text{so}}\epsilon_r)_{\text{GaAs}}}\right)^2 \approx 10^{-6}. \tag{B4}$$

Here p is the fraction of the isotope ^{29}Si. We have found previously that in a GaAs quantum dot with parameters typical in experiments, the nuclear dominance requires exchange energies of the order of 0.1 μeV. As follows from Eq. (B4), in silicon the requirements are much more stringent and thus it is less suitable for such an effect demonstration. The reason for this is the different material parameters, most importantly the much weaker coupling of the conduction electrons to the nuclear spins and the low fraction of atoms with nonzero nuclear magnetic moment in silicon.

[1] D. Loss and D. P. DiVincenzo, Phys. Rev. A **57**, 120 (1998).
[2] S. A. Wolf, D. D. Awschalom, R. A. Buhrman, J. M. Daughton, S. von Molnr, M. L. Roukes, A. Y. Chtchelkanova, and D. M. Treger, Science **294**, 1488 (2001).
[3] I. Žutić, J. Fabian, and S. Das Sarma, Rev. Mod. Phys. **76**, 323 (2004).
[4] J. Fabian, A. Matos-Abiague, C. Ertler, P. Stano, and I. Žutić, Acta Phys. Slov. **57**, 565 (2007).
[5] M. A. Nielsen and I. L. Chuang, *Quantum Computation and Quantum Information* (Cambridge University Press, Cambridge, 2000).
[6] A. Barenco, C. H. Bennett, R. Cleve, D. P. DiVincenzo, N. Margolus, P. Shor, T. Sleator, J. A. Smolin, and H. Weinfurter, Phys. Rev. A **52**, 3457 (1995).
[7] D. P. DiVincenzo, Fortschr. Phys. **48**, 771 (2000).
[8] T. D. Ladd, F. Jelezko, R. Laflamme, Y. Nakamura, C. Monroe, and J. L. O'Brien, Nature (London) **464**, 45 (2010).
[9] R. Hanson, L. P. Kouwenhoven, J. R. Petta, S. Tarucha, and L. M. K. Vandersypen, Rev. Mod. Phys. **79**, 1217 (2007).
[10] R. Brunner, Y.-S. Shin, T. Obata, M. Pioro-Ladrière, T. Kubo, K. Yoshida, T. Taniyama, Y. Tokura, and S. Tarucha, Phys. Rev. Lett. **107**, 146801 (2011).
[11] J. M. Taylor, J. R. Petta, A. C. Johnson, A. Yacoby, C. M. Marcus, and M. D. Lukin, Phys. Rev. B **76**, 035315 (2007).
[12] E. A. Laird, C. Barthel, E. I. Rashba, C. M. Marcus, M. P. Hanson, and A. C. Gossard, Phys. Rev. Lett. **99**, 246601 (2007).
[13] M. Pioro-Ladriere, T. Obata, Y. Tokura, Y.-S. Shin, T. Kubo, K. Yoshida, T. Taniyama, and S. Tarucha, Nat. Phys. **4**, 776 (2008).
[14] J. R. Petta, A. C. Johnson, J. M. Taylor, E. A. Laird, A. Yacoby, M. D. Lukin, C. M. Marcus, M. P. Hanson, and A. C. Gossard, Science **309**, 2180 (2005).
[15] T. Meunier, V. E. Calado, and L. M. K. Vandersypen, Phys. Rev. B **83**, 121403 (2011).
[16] F. H. L. Koppens, C. Buizert, K. J. Tielrooij, I. T. Vink, K. C. Nowack, T. Meunier, L. P. Kouwenhoven, and L. M. K. Vandersypen, Nature (London) **442**, 766 (2006).
[17] K. C. Nowack, F. H. L. Koppens, Y. V. Nazarov, and L. M. K. Vandersypen, Science **318**, 1430 (2007).
[18] S. Foletti, H. Bluhm, D. Mahalu, V. Umansky, and A. Yacoby, Nat. Phys. **5**, 903 (2009).
[19] A. V. Khaetskii and Y. V. Nazarov, Phys. Rev. B **64**, 125316 (2001).
[20] J. Schliemann, A. Khaetskii, and D. Loss, J. Phys.: Condens. Matter **15**, R1809 (2003).
[21] J. R. Petta, J. M. Taylor, A. C. Johnson, A. Yacoby, M. D. Lukin, C. M. Marcus, M. P. Hanson, and A. C. Gossard, Phys. Rev. Lett. **100**, 067601 (2008).
[22] M. S. Rudner and L. S. Levitov, Phys. Rev. Lett. **99**, 246602 (2007).
[23] A. Imamoglu, E. Knill, L. Tian, and P. Zoller, Phys. Rev. Lett. **91**, 017402 (2003).
[24] D. Stepanenko, G. Burkard, G. Giedke, and A. Imamoglu, Phys. Rev. Lett. **96**, 136401 (2006).
[25] F. H. L. Koppens, J. A. Folk1, J. M. Elzerman, R. Hanson, L. H. W. van Beveren, I. T. Vink, H. P. Tranitz, W. Wegscheider, L. P. Kouwenhoven, and L. M. K. Vandersypen, Science **309**, 1346 (2005).
[26] I. T. Vink, K. C. Nowack, F. H. L. Koppens, J. Danon, Y. V. Nazarov, and L. M. K. Vandersypen, Nat. Phys. **5**, 764 (2009).
[27] G. Balasubramanian, P. Neumann, D. Twitchen, M. Markham, R. Kolesov, N. Mizuochi, J. Isoya, J. Achard, J. Beck, J. Tissler, V. Jacques, P. R. Hemmer, F. Jelezko, and J. Wrachtrup, Nat. Mater. **8**, 383 (2009).
[28] T. D. Ladd, D. Maryenko, Y. Yamamoto, E. Abe, and K. M. Itoh, Phys. Rev. B **71**, 014401 (2005).
[29] J. J. L. Morton, D. R. McCamey, M. A. Eriksson, and S. A. Lyon, Nature (London) **479**, 345 (2011).
[30] J. W. Ager and E. E. Haller, Phys. Status Solidi A **203**, 3550 (2006).
[31] J. Sailer, V. Lang, G. Abstreiter, G. Tsuchiya, K. M. Itoh, J. W. Ager, E. E. Haller, D. Kupidura, D. Harbusch, S. Ludwig, and D. Bougeard, Phys. Status Solidi RRL **3**, 61 (2009).
[32] A. Wild, J. Kierig, J. Sailer, J. W. Ager, III, E. E. Haller, G. Abstreiter, S. Ludwig, and D. Bougeard, Appl. Phys. Lett. **100**, 143110 (2012).
[33] M. G. Borselli, K. Eng, E. T. Croke, B. M. Maune, B. Huang, R. S. Ross, A. A. Kiselev, P. W. Deelman, I. Alvarado-Rodriguez, A. E. Schmitz, M. Sokolich, K. S. Holabird, T. M. Hazard, M. F. Gyure, and A. T. Hunter, Appl. Phys. Lett. **99**, 063109 (2011).
[34] B. M. Maune, M. G. Borselli, B. Huang, T. D. Ladd, P. W. Deelman, K. S. Holabird, A. A. Kiselev, I. Alvarado-Rodriguez, R. S. Ross, A. E. Schmitz, M. Sokolich, C. A. Watson, M. F. Gyure, and A. T. Hunter, Nature (London) **481**, 344 (2012).

[35]J. R. Prance, Z. Shi, C. B. Simmons, D. E. Savage, M. G. Lagally, L. R. Schreiber, L. M. K. Vandersypen, M. Friesen, R. Joynt, S. N. Coppersmith, and M. A. Eriksson, Phys. Rev. Lett. **108**, 046808 (2012).
[36]E. P. Nordberg, G. A. Ten Eyck, H. L. Stalford, R. P. Muller, R. W. Young, K. Eng, L. A. Tracy, K. D. Childs, J. R. Wendt, R. K. Grubbs, J. Stevens, M. P. Lilly, M. A. Eriksson, and M. S. Carroll, Phys. Rev. B **80**, 115331 (2009).
[37]M. A. Eriksson, M. Friesen, S. N. Coppersmith, R. Joynt, L. J. Klein, K. Slinker, C. Tahan, P. M. Mooney, J. O. Chu, and S. J. Koester, Quantum Inf. Proc. **3**, 133 (2004).
[38]F. Schäffler, Semicond. Sci. Technol. **12**, 1515 (1997).
[39]D. J. Paul, Semicond. Sci. Technol. **19**, R75 (2004).
[40]M. S. Dresselhaus, G. Dresselhaus, and A. Jorio, *Group Theory: Application to the Physics of Condensed Matter*, 1st ed. (Springer, Berlin, 2008).
[41]T. Ando, A. B. Fowler, and F. Stern, Rev. Mod. Phys. **54**, 437 (1982).
[42]T. Ando, Phys. Rev. B **19**, 3089 (1979).
[43]P. Weitz, R. Haug, K. von. Klitzing, and F. Schäffler, Surf. Sci. **361-362**, 542 (1996).
[44]S. Goswami, K. A. Slinker, M. Friesen, L. M. McGuire, J. L. Truitt, C. Tahan, L. J. Klein, J. O. Chu, P. M. Mooney, D. W. van der Weide, R. Joynt, S. N. Coppersmith, and M. A. Eriksson, Nat. Phys. **3**, 41 (2007).
[45]A. L. Saraiva, M. J. Calderón, X. Hu, S. Das Sarma, and B. Koiller, Phys. Rev. B **80**, 081305 (2009).
[46]D. Culcer, L. Cywiński, Q. Li, X. Hu, and S. Das Sarma, Phys. Rev. B **82**, 155312 (2010).
[47]M. Friesen, S. Chutia, C. Tahan, and S. N. Coppersmith, Phys. Rev. B **75**, 115318 (2007).
[48]M. Friesen and S. N. Coppersmith, Phys. Rev. B **81**, 115324 (2010).
[49]M. G. Borselli, R. S. Ross, A. A. Kiselev, E. T. Croke, K. S. Holabird, P. W. Deelman, L. D. Warren, I. Alvarado-Rodriguez, I. Milosavljevic, F. C. Ku, W. S. Wong, A. E. Schmitz, M. Sokolich, M. F. Gyure, and A. T. Hunter, Appl. Phys. Lett. **98**, 123118 (2011).
[50]D. Culcer, L. Cywinski, Q. Li, X. Hu, and S. Das Sarma, Phys. Rev. B **80**, 205302 (2009).
[51]Q. Li, L. Cywinski, D. Culcer, X. Hu, and S. Das Sarma, Phys. Rev. B **81**, 085313 (2010).
[52]N. S. Lai, W. H. Lim, C. H. Yang, F. A. Zwanenburg, W. A. Coish, F. Qassemi, A. Morello, and A. S. Dzurak, Sci. Rep. **1**, 110 (2011).
[53]R. R. Hayes, A. A. Kiselev, M. G. Borselli, S. S. Bui, E. T. Croke III, P. W. Deelman, B. M. Maune, I. Milosavljevic, J. Moon, R. S. Ross, A. E. Schmitz, M. F. Gyure, and A. T. Hunter, arXiv:0908.0173.
[54]C. B. Simmons, J. R. Prance, B. J. Van Bael, T. S. Koh, Z. Shi, D. E. Savage, M. G. Lagally, R. Joynt, M. Friesen, S. N. Coppersmith, and M. A. Eriksson, Phys. Rev. Lett. **106**, 156804 (2011).
[55]D. Culcer, A. L. Saraiva, B. Koiller, X. Hu, and S. Das Sarma, Phys. Rev. Lett. **108**, 126804 (2012).
[56]M. Xiao, M. G. House, and H. W. Jiang, Phys. Rev. Lett. **104**, 096801 (2010).
[57]W. Pan, X. Z. Yu, and W. Z. Shen, Appl. Phys. Lett. **95**, 013103 (2009).
[58]A. Tyryshkin, S. Lyon, T. Schenkel, J. Bokor, J. Chu, W. Jantsch, F. Schäffler, J. Truitt, S. Coppersmith, and M. Eriksson, Physica E **35**, 257 (2006).
[59]C. Tahan, M. Friesen, and R. Joynt, Phys. Rev. B **66**, 035314 (2002).
[60]M. Prada, R. H. Blick, and R. Joynt, Phys. Rev. B **77**, 115438 (2008).
[61]B. A. Glavin and K. W. Kim, Phys. Rev. B **68**, 045308 (2003).
[62]M. Raith, P. Stano, and J. Fabian, Phys. Rev. B **83**, 195318 (2011).
[63]L. Wang and M. W. Wu, J. Appl. Phys. **110**, 043716 (2011).
[64]L. Wang, K. Shen, B. Y. Sun, and M. W. Wu, Phys. Rev. B **81**, 235326 (2010).
[65]K. Shen and M. W. Wu, Phys. Rev. B **76**, 235313 (2007).
[66]E. Y. Sherman and D. J. Lockwood, Phys. Rev. B **72**, 125340 (2005).
[67]F. A. Zwanenburg, A. S. Dzurak, A. Morello, M. Y. Simmons, L. C. L. Hollenberg, G. Klimeck, S. Rogge, S. N. Coppersmith, and M. A. Eriksson, arXiv:1206.5202.
[68]J. Fabian and S. Das Sarma, Phys. Rev. Lett. **81**, 5624 (1998).
[69]M. Raith, P. Stano, F. Baruffa, and J. Fabian, Phys. Rev. Lett. **108**, 246602 (2012).
[70]P. Stano and J. Fabian, Phys. Rev. Lett. **96**, 186602 (2006).
[71]M. Raith, Diploma thesis, University of Regensburg, Germany, 2009.
[72]J. Pedersen, C. Flindt, N. A. Mortensen, and A.-P. Jauho, Phys. Rev. B **76**, 125323 (2007).
[73]P. Stano and J. Fabian, Phys. Rev. B **77**, 045310 (2008).
[74]Y. A. Bychkov and E. I. Rashba, J. Phys. C **17**, 6039 (1984).
[75]G. Dresselhaus, Phys. Rev. **100**, 580 (1955).
[76]L. E. Golub and E. L. Ivchenko, Phys. Rev. B **69**, 115333 (2004).
[77]M. O. Nestoklon, E. L. Ivchenko, J.-M. Jancu, and P. Voisin, Phys. Rev. B **77**, 155328 (2008).
[78]L. V. C. Assali, H. M. Petrilli, R. B. Capaz, B. Koiller, X. Hu, and S. Das Sarma, Phys. Rev. B **83**, 165301 (2011).
[79]A. Khaetskii, D. Loss, and L. Glazman, Phys. Rev. B **67**, 195329 (2003).
[80]I. A. Merkulov, A. L. Efros, and M. Rosen, Phys. Rev. B **65**, 205309 (2002).
[81]C. Herring and E. Vogt, Phys. Rev. **101**, 944 (1956).
[82]H. Hasegawa, Phys. Rev. **118**, 1523 (1960).
[83]E. Pop, R. W. Dutton, and K. E. Goodson, J. Appl. Phys. **96**, 4998 (2004).
[84]M. Dür, A. D. Gunther, D. Vasileska, and S. M. Goodnick, Nanotechnology **10**, 142 (1999).
[85]A. Grodecka, L. Jacak, P. Machnikowski, and K. Roszak, *Quantum Dots: Research Developments* (Nova Science, New York, 2005).
[86]F. Baruffa, P. Stano, and J. Fabian, Phys. Rev. Lett. **104**, 126401 (2010); Phys. Rev. B **82**, 045311 (2010).
[87]L. Yang, J. R. Watling, R. C. W. Wilkins, M. Borii, J. R. Barker, A. Asenov, and S. Roy, Semicond. Sci. Technol. **19**, 1174 (2004).
[88]M. M. Rieger and P. Vogl, Phys. Rev. B **48**, 14276 (1993).
[89]H. Malissa, W. Jantsch, M. Muhlberger, F. Schaffler, Z. Wilamowski, M. Draxler, and P. Bauer, Appl. Phys. Lett. **85**, 1739 (2004).
[90]*Semiconductors: Group IV Elements, IV-IV and III-V Compounds*, edited by O. Madelung, U. Rössler, and M. Schulz, Landolt-Börnstein, New Series, Group III, Vol. 41, Pt. A1b (Springer, Berlin, 2002).
[91]M. V. Fischetti and S. E. Laux, J. Appl. Phys. **80**, 2234 (1996).
[92]D. S. Gandolfo, D. A. Williams, and H. Qin, J. Appl. Phys. **97**, 063710 (2005).
[93]V. N. Golovach, A. Khaetskii, and D. Loss, Phys. Rev. Lett. **93**, 016601 (2004).

[94]P. Stano and J. Fabian, Phys. Rev. B **74**, 045320 (2006).
[95]U. Merkt, J. Huser, and M. Wagner, Phys. Rev. B **43**, 7320 (1991).
[96]L. P. Gorkov and P. L. Krotkov, Phys. Rev. B **68**, 155206 (2003).
[97]P. Löwdin, J. Chem. Phys. **19**, 1396 (1951).
[98]J. R. Schrieffer and P. A. Wolff, Phys. Rev. **149**, 491 (1966).
[99]R. Winkler, *Spin-Orbit Coupling Effects in Two-Dimensional Electron and Hole Systems*, 1st ed. (Springer, Berlin, 2003).
[100]W. Heitler and F. London, Z. Phys. **44**, 455 (1927).
[101]P. Stano and J. Fabian, Phys. Rev. B **72**, 155410 (2005).
[102]G. Burkard, D. Loss, and D. P. DiVincenzo, Phys. Rev. B **59**, 2070 (1999).